Evaluation of Perovskite Photo-sensors with Electron-beam Evaporated Titanium Dioxide Films

M. F. Hossain,[1,2] I. Hirano,[1] S. Naka,[1] and H. Okada[1]

[1]University of Toyama, Graduate School of Science & Engineering,
3190 Gofuku, Toyama 930-8555, Japan.
Phone: +81-76-445-6730 Fax: +81-76-445-6732 E-mail: okada@eng.u-toyama.ac.jp
[2]Rajshahi University of Engineering & Technology, Department of Electrical and Electronic Engineering
Rajshahi-6204, Bangladesh.

We have investigated a perovskite photo-sensors with electron-beam evaporated titanium dioxide (TiO_2) film as an electron transport buffer layer. The TiO_2 films have been deposited on indium-doped tin oxide (ITO) glass substrate at room temperature. Then, prepared TiO_2 films are annealed at different temperatures of between room temperature and 500°C. Device structure is ITO/ TiO_2/ Perovskite layer/ 2,2,7,7-tetrakis (N,N-di-p-methoxyphenylamine)-9,9-spirobifluorene/ Au. Before and after annealing process, TiO_2 films have changed from an amorphous to crystalline structure mixed with anatase and rutile phases. For a sensing characteristics, a ratio of photo- and dark-current was 1.1×10^3 without annealing condition. It is assumed that a flat device structure and a larger photocurrent under illumination are effective to reduce carrier generation site.

1. Introduction

Organic electronic devices, such as an organic light emitting diodes (OLEDs),[1-3] an organic thin-film transistors (OTFTs),[4-8] an organic sensing devices[9-11] and an organic solar cells (OSCs)[12-15] are widely studied. Especially in OSCs, one of the most interesting topics is an organic-inorganic hybrid perovskite solar cell (PeSC) that have considered as an alternative photovoltaic technology due to their excellent photoelectric conversion efficiency (PCE) along with their low material costs, and its recorded power conversion efficiency of 23.7%.[16] A compact titanium dioxide (TiO_2) layer is the most promising electron-transport layer for the PeSC.[15] For achieving the higher efficiency PeSCs with a suitable electronic property of TiO_2, several methods such as sol−gel, spin-coating, slot-die coating, blade coating, electrodeposition, atomic layer deposition, and electron beam evaporation (EBE) have been used.[17-19] Among these methodologies, the EBE is one of the most attractive techniques because it is common, versatile and inexpensive which can produce TiO_2 films with good optical and mechanical properties.[20,21] In our previous study, the TiO_2 photoelectrode has been prepared on an ITO substrate by the EBE system at room temperature (RT). After that, prepared TiO_2 films are annealed at different temperatures of 150~500°C. The effect of annealing temperature on the structural, optical, and surface morphological properties of ITO/TiO_2 and ITO/TiO_2/ perovskite (Pe) structures have been correlated and discussed with their photovoltaic performance of PeSCs.[22] This larger photo-current is suitable for photo-sensors. In this paper, we have investigated the preliminary evaluation of organic-related perovskite photo-sensors (PePS) by applying reverse-biased voltage to collect the photo-generated carrier for light sensing applications.

2. Experiment

Fabrication of the thin film, evaluation of a physical nature of the TiO_2 thin film, device fabrication, and measurement setup are virtually identical to that of our previous PeSC experiment.[22] Details are as follows. First, the ITO glass substrates were etched by photolithography and were thoroughly cleaned using the process of ultra-sonication, and irradiation in an UV-ozone chamber. Then, the EBE was carried out. Initially, the chamber was evacuated to a background pressure below 4×10^{-6} Torr. The TiO_2 films were evaporated on the ITO substrate by EBE system at RT. The film thicknesses of all TiO_2 films were around 300 nm measured by computer-controlled quartz crystal microbalance (QCM) apparatus. The prepared TiO_2 thin films were annealed with different temperatures of 150~500°C for 1 h. The perovskite layer was deposited on TiO_2 thin films by the two-step method in the glovebox with an N_2 environment. Perovskite precursor solutions were prepared by dissolving PbI_2 (Aldrich, 99% purity) in anhydrous N,N-dimethylformamide (400 mg/mℓ) and methyl-ammonium iodide (MAI) (Aldrich) in ethanol (50 mg/mℓ, 19:1 ratio). First of all, PbI_2 was depositing on prepared ITO/TiO_2 films

by the spin-coating method at 3,000 rpm under N_2 environment. Then, a single-drop (80 μℓ) of MAI solution was added and again spinning at 3,000 rpm. Finally, the perovskite-coated TiO_2 electrode was heated with 100°C for 10 min. The 2,2,7,7-tetrakis (N,N-di-p-methoxyphenylamine)-9,9-spirobifluorene(Spiro-OMeTAD) solution was prepared by dissolving 72.3 mg of Spiro-OMeTAD (Aldrich, 99% purity), 17.5 μℓ of lithium bis (trifluoromethane-sulfonyl) imide (LITFSI, Wako, 99.95%) solution (520 mg of LITSFI in 1 mℓ acetonitrile (Aldrich, 99.8%)) and 28.8 μℓ of 4-tert-butylpyridine (Aldrich, 96%) in 1 mℓ of chlorobenzene (Aldrich, 99.8%). This hole-transport layer was deposited on top of the ITO/TiO_2/perovskite substrate by spin-coating at 4,000 rpm in air. Finally, a 50 nm thick gold metal was evaporated with an evaporation rate of 1.0 Å/s.

The surface morphologies were investigated using field emission scanning electron microscope (FE-SEM, JEOL 6700F). The crystal structure of the TiO_2 and TiO_2/perovskite layer were examined by X-ray diffractometer (XRD, Bruker Discover 8) analysis with Cu-Kα line. The optical properties of the films were measured by UV/VIS spectrophotometer (Hitachi U-1900) at RT within the wavelength range 300-900 nm. The photo-sensing characteristics of the PePSs were measured using a semiconductor parameter analyzer (KEYSIGHT, B1500A) and solar simulator AM 1.5 (Yamashita Denso, YSS E40). The IPCE spectra were measured using a motor-controlled monochromator (Shimadzu, SPG-100ST, AT-100PCC, and AT- 100PL), a halogen lamp (Scott, MegaLight 100), and a digital electrometer (Advantest, TR8652). The IPCE was calibrated using a Si photodiode (Hamamatsu Photonics, S1223).

3. Results and Discussions

Before evaluating the device characteristics, sheet resistance of ITO, surface morphologies of ITO/TiO_2, and ITO/TiO_2/Pe structure were evaluated.[22] The sheet resistance is increased slowly from 11.1 to 20.4 Ω/□ with the increase of annealing temperature from RT to 250°C, respectively. However, these resistances have become high from 58.2 to 78.9 Ω/□ due to increasing the annealing temperature of 350~500°C. The change of resistance may be happened by the decrease of electron concentration.[23-25]

The surface morphology of TiO_2 annealed at different temperatures of RT, 150, 250, 350, 400, 450, and 500°C, cross-sectional view of TiO_2 thin films at RT, and Pe/RT and Pe/500°C are shown in Figs. 1(a)-1(g), Fig. 1(h), and Figs. 1(i)-1(j), respectively.[22] In the Fig. 1(a), the TiO_2 prepared at RT shows very smooth and compact without the open surface. The grain boundaries of TiO_2 films are become visible after annealing with the temperature of 150~500°C. From Figs. 1(b)-(g), the surface of TiO_2 films has become porous with the more open surface with the increase of annealing temperature. The grain-cluster size is increased between 17.2 and 37.1 nm with the temperature between 150 and 500°C, respectively. This is because increasing the annealing temperature leads to increase the crystallinity of the material and hence increases the number of crystallites, which exhibits similar behavior as discussed in XRD analysis. Figure 1(h) displays the cross-sectional view of TiO_2 at RT. It is cleared that the measured thickness of TiO_2 is 300 nm, which is the same thickness as measured by the QCM during the TiO_2 evaporation.

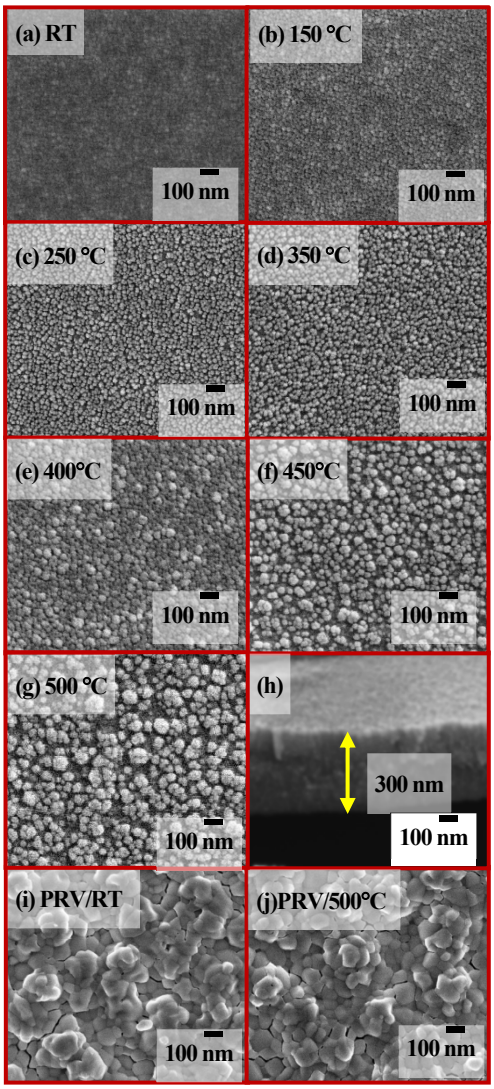

Fig. 1 FE-SEM images for TiO_2 thin films annealed at (a) RT, (b) 150°C, (c) 250°C (d) 350°C (e) 400°C (f) 450°C, and (g) 500°C, (h) cross-section of TiO_2 films at RT, (i) TiO_2 /Pe at RT, and (j) TiO_2/Pe at 500°C annealing temperature.[22]

From Figs. 1(i)-1(j), it is clearly observed that the surface of Pe/RT and Pe/500°C has almost the same structure and compact with closely bounded grains.

From an absorption measurements, the band gap of the TiO_2 film decreases from 3.31 to 3.10 eV with the increase of annealing temperature from RT to 500°C, respectively. The decreasing the band gap indicates that the photoactivity TiO_2 is also increased. However, the band gap of TiO_2 is larger than the perovskite band gap.[26] Therefore, this optical properties of TiO_2 is no influenced on the absorption of perovskite layer.

The succeeding device fabrication procedure was carried out at a low temperature of below 150°C. A cross-sectional SEM image of PePS with TiO_2 films prepared at RT is confirmed. The ITO, TiO_2, perovskite, Spiro-OMeTAD and Au layer are clearly observed. The average thickness of perovskite and Spiro-OMeTAD are approximately 400 and 350 nm, respectively.

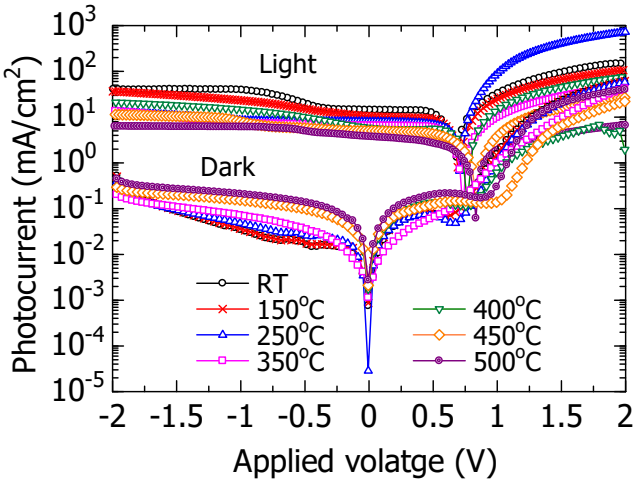

Fig. 2 Photo-sensing characteristics with different temperature of TiO_2 annealing conditions.

The photo-sensing characteristics with different temperature of TiO_2 annealing conditions are shown in Fig. 2. By increasing the annealing temperature, photocurrent under light illumination was decreased, while the dark current was gradually increased. Under forward biased condition, magnitude relations are identical below an open circuit voltage (V_{OC}) of that of the solar cell characteristics. By applying further forward-biased conditions between V_{OC} and +2 V, the dark current was increased in a similar to diode configuration, while the photocurrent was little larger than that of the revise-biased conditions.

Measured PePS characteristics are shown in Table I. The PeSC characteristics are also estimated that are not shown in this table.

Table I. Photo-sensing characteristics with TiO_2 thin films at different annealing temperatures.

Annealing temperature (°C)	I_{dark} (mA/cm^2)	I_{photo} (mA/cm^2)	I_{photo}/I_{dark}
RT	3.47×10^{-2}	39	1.12×10^{3}
150	3.61×10^{-2}	23.3	6.45×10^{2}
250	4.76×10^{-2}	8.59	1.80×10^{2}
350	7.10×10^{-2}	7.37	1.04×10^{2}
400	0.174	14.7	84.5
450	0.153	7.94	51.9
500	0.209	6.11	29.2

A ratio of photo- and dark-current was 1.1×10^3 for the PePS without annealing condition. This current ratio is the best value for different TiO_2 annealing temperature and gradually decreased with increase in the annealing temperature because of the decrease of photocurrent and increase of dark current.

Let us discuss a description of the device operations and models. First, the difference of photocurrent is discussed. The ITO resistance was increased with increase in the annealing temperature. This is primary reason why the photo current in the device without annealing was larger than that of TiO_2 annealing. Next, the difference of dark current is also discussed. As shown in Fig. 1, smoother surface morphology was obtained for the case without TiO_2 annealing condition. By increasing the annealing temperature, roughness and grain size of TiO_2 layer were increased. After the coating of perovskite layer, on the other hands, the roughness, grain size, and formation of small cracks seemed to identical, as seen in Figs. 1(i) and 1(j). According to a departure from the ideal p-n junction under reverse-biased voltage is mainly due to the generation current in the depletion region by[27]

$$J_{gen} = \frac{qn_iW}{\tau_e}, \qquad (2)$$

where, W is the depletion-layer width, τ_e is the effective lifetime, q is the unit charge, and n_i is the intrinsic carrier concentration. The effective life time is largely depends on a trap behavior that arises from a dangling bond around the grain of semiconductor. In the case of this perovskite photo-sensor, grain condition of the perovskite-layer seems to be identical within the SEM observation. If we consider that the perovskite crystal is the same, it is assumed that primary difference of the PePS characteristics with different annealing temperature is arises from the interfacial defects at TiO_2/perovskite layers and TiO_2 thin film itself, where, traps and some crystal defects induce the generation current. As a result, dark current of the PePS was increased.

4. Conclusions

We had investigated the perovskite photo-sensors with electron-beam evaporated TiO_2 film as the electron transport buffer layer. Obtained maximum current ratio of photo- and dark-current was 1.1×10^3 without annealing condition. Further consideration is necessary in order to reduce the generation current and improve the PePS characteristics.

Acknowledgments

Md. Faruk Hossain would like to thank the Japanese Society for Promotion of Science (JSPS) for the fellowship and the financial assistance (MEXT/JSPS KAKENHI Grant Number: JP16F16372).

References

1) C. W. Tang and S. A. VanSlyke, Appl. Phys. Lett. **51**, 913 (1987).

2) C. Adachi et al., Appl. Phys. Lett. **90**, 5048 (2001).

3) A. Endo et al., Adv. Mater. **21**, 4802 (2009).

4) K. Kudo et al., Jpn. J. Appl. Phys. **23**, 130 (1984).

5) A. Tsumura et al., Appl. Phys. Lett. **49**, 1210 (1986).

6) Y. -Y. Lin et al., IEEE Trans. Electron Devices, **44**, 1325 (1997).

7) T. Hyodo et al., Jpn. J. Appl. Phys. **43**, 2323 (2004).

8) M. Katsuhara et al, J. SID **18**, 399 (2010).

9) G. Yu et al., Adv. Mater. **10**, 1431 (1998).

10) T. N. Ng et al., Appl. Phys. Lett. **92**, 213303 (2008).

11) T. Zukawa et al., J. Appl. Phys. **91**, 1171 (2002).

12) C. W. Tang, Appl. Phys. Lett. **48**, 183 (1986).

13) G. Yu and A. J. Heeger, J. Appl. Phys. **78**, 4510 (1995).

14) L. Meng et al., Science **361**, 1094 (2018).

15) A. Kojima at al., J. Am. Chem. Soc. **131**, 6050 (2009).

16) NREL: https://www.nrel.gov/pv/cell-efficiency.html.

17) D. M. -Rojas et al., Progr. Photovoltaics **21**, 393 (2013).

18) H. C. Weerasinghe et al., J. Photochem. Photobiol. A **213**, 30 (2010).

19) J. Gong et al., Renew. Sust. Energy Rev. **16**, 5848 (2012).

20) S. H. Oh et al., Mater. Letts. **57**, 4151 (2003).

21) W. Qiu et al., J. Mater. Chem. A, **3**, 22824 (2015).

22) M. F. Hossain et al., J. Photochemistry & Photobiology A: Chemistry **360**, 109 (2018).

23) N. Nishimoto et al., Phys. Status Solidi A, **210**, 589 (2013).

24) N. Nishimoto et al., J. Cryst. Growth **310**, 5003 (2008).

25) C. M. Chen et al., J. Alloys Compd. **509**, 872 (2011).

26) L. Etgar et al., J. Am. Chem. Soc. **134**, 17396 (2012).

27) S. M. Sze, Physics of Semiconductor Devices, John Wiley & Sons, New York, 644 (1981).